






RESEARCH ARTICLE | JANUARY 23 2023

Sequence-specific binding behavior of coralyne toward triplex DNA: An ultrafast time-resolved fluorescence spectroscopy study

Zeqing Jiao ; Chunfan Yang; Qian Zhou; Zheng Hu; Jialong Jie  ; Xianwang Zhang; Hongmei Su  



J. Chem. Phys. 158, 045101 (2023)

<https://doi.org/10.1063/5.0133913>

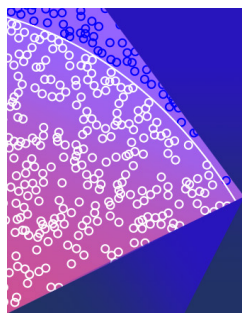


View
Online



Export
Citation

CrossMark



The Journal of Chemical Physics

Special Topic: Monte Carlo methods,
70 years after Metropolis *et al.* (1953)

Submit Today

Sequence-specific binding behavior of coralyne toward triplex DNA: An ultrafast time-resolved fluorescence spectroscopy study

Cite as: J. Chem. Phys. 158, 045101 (2023); doi: 10.1063/5.0133913

Submitted: 7 November 2022 • Accepted: 4 January 2023 •

Published Online: 23 January 2023



View Online



Export Citation



CrossMark

Zeqing Jiao,¹ Chunfan Yang, Qian Zhou, Zheng Hu, Jialong Jie,^{a)} Xianwang Zhang, and Hongmei Su^{a)}

AFFILIATIONS

College of Chemistry, Beijing Normal University, Beijing 100875, People's Republic of China

^{a)} Authors to whom correspondence should be addressed: jialong@bnu.edu.cn and hongmei@bnu.edu.cn

ABSTRACT

Triplex DNA structure has potential therapeutic application in inhibiting the expression of genes involved in cancer and other diseases. As a DNA-targeting antitumor and antibiotic drug, coralyne shows a remarkable binding propensity to triplex over canonical duplex and thus can modulate the stability of triplex structure, providing a prospective gene targeting strategy. Much less is known, however, about coralyne-binding interactions with triplex. By combining multiple steady-state spectroscopy with ultrafast fluorescence spectroscopy, we have investigated the binding behaviors of coralyne with typical triplexes. Upon binding with a G-containing triplex, the fluorescence of coralyne is markedly quenched owing to the photoinduced electron transfer (PET) of coralyne with the G base. Systematic studies show that the PET rates are sensitive to the binding configuration and local microenvironment, from which the coexisting binding modes of monomeric (full and partial) intercalation and aggregate stacking along the sugar-phosphate backbone are distinguished and their respective contributions are determined. It shows that coralyne has preferences for monomeric intercalation within CGG triplex and pure TAT triplex, whereas CGC⁺ triplex adopts mainly backbone binding of coralyne aggregates due to charge repulsion, revealing the sequence-specific binding selectivity. The triplex-DNA-induced aggregation of coralyne could be used as a probe for recognizing the water content in local DNA structures. The strong π - π stacking of intercalated coralyne monomer with base-triplets plays an important role in stabilizing the triplex structure. These results provide mechanistic insights for understanding the remarkable propensity of coralyne in selective binding to triplex DNA and shed light on the prospective applications of coralyne-triplex targeted anti-gene therapeutics.

Published under an exclusive license by AIP Publishing. <https://doi.org/10.1063/5.0133913>

I. INTRODUCTION

Non-B DNA structures, such as G-quadruplex, triplex DNA, i-Motif, Z-DNA, and so forth, are attracting increasing attention owing to their important roles in many biological processes.^{1,2} The formation of these unusual secondary structures is associated with genetic instability and can consequently cause human diseases.^{3,4} Among these non-B DNA types, triplex DNA is a family of triple helical structures formed at mirror repeat regions, where a single-stranded triplex-forming oligonucleotide winds back and binds in the major groove of target duplex DNA via Hoogsteen hydrogen bonding.^{5,6} Previous studies have demonstrated that triplex DNA has potential therapeutic application in inhibiting the expression of genes involved in cancer and other human diseases, either by targeting disease genes for inactivation, stimulating DNA repair

and/or homologous recombination pathways, inducing site-specific mutations, or interfering with DNA replication.⁷ However, the binding of the Hoogsteen base-paired third strand is weak compared to Watson-Crick pairing, resulting in low stability of the triplex and thus limiting their application *in vivo*.^{8,9} Intriguingly, small molecules (so-called ligands) can bind triplex DNA and stabilize triplex DNA conformation, which presents a prospective gene targeting strategy.⁷⁻¹¹ These triplex ligands are thus important because of their promising use as a gene targeting strategy, and great interest has been sparked in the synthetic design of ligand structures and the understanding of interactions between ligands and triplex DNA.¹⁰⁻¹⁴

The cationic ligand coralyne (Scheme 1) has been of particular interest because it can target and bind with DNA/RNA structures and show a wide range of clinical effects, including anti-tumor,

anti-inflammation, anti-microbe, anti-leukemia, and anti-malaria.^{15–20} Coralyne consists of an extended aromatic ring system and has a greater surface area analogous to triplex base-triplets (namely, the base-pair in triplex), thus exhibiting a remarkable propensity for binding the triplex DNA than other DNA structures.^{14,21} By Scatchard analysis of steady-state fluorescence quenching, Lee *et al.* reported that the binding of coralyne with triplex DNA involves biphasic binding modes of monomeric intercalation within two neighboring base-triplets and aggregate stacking along DNA negative phosphate backbone.¹⁴ Later, based on steady-state measurements [UV-Vis, melting temperature, DNase I footprinting, nuclear magnetic resonance (NMR) spectra, etc.], Moraru-Allen *et al.* proposed a partial intercalation mode for coralyne binding to triplexes containing pyrimidine-purine-pyrimidine (CGC⁺) segments, which is a weaker binding mode than the fully intercalated mode of coralyne within the TAT triplex.^{16,22} However, current methods are generally sensitive to only one type of binding mode and it is thus difficult to simultaneously distinguish different ones in a single measurement.

Moreover, for coralyne bound with a triplex containing pyrimidine-purine-pyrimidine (CGC⁺) segments, although studied by various methods, its binding mode is still controversial, with no consensus to date.^{14,16,22} Lee *et al.* suggested that coralyne showed little sequence specificity for triplex and bound tightly to triplex with and without CGC⁺ segments.¹⁴ The explanation was that for coralyne, the positive charge is most localized on the aromatic ring, and less charge will be delocalized onto the methoxy groups, which are actually in closer proximity to the protonated cytosine if coralyne is intercalated. Owing to such a charge distribution, the electrostatic repulsion between coralyne and protonated cytosine was thought not strong enough to affect the intercalation of coralyne in a triplex with CGC⁺ segments, and thus there was no binding preference for two triplexes. Nevertheless, in the later studies, Moraru-Allen *et al.* showed that coralyne had a preferential intercalation for pure TAT triplex compared with triplex with alternating TAT and CGC⁺ segments.²² For CGC⁺-containing triplex, coralyne may only partially intercalate into base-triplets, as a consequence of long range electrostatic repulsion between positively charged ligand and the protonated cytosine. Thus, an intriguing question lies in whether the interactions of coralyne with CGC⁺-containing triplex are affected by the electrostatic repulsion and whether the binding behavior is sequence-specific. In this context, recognizing a full scenario of mixed binding modes and further quantifying their respective contributions is highly desirable for understanding the complicated interactions of coralyne with triplex DNA.

In pursuing answers to these questions, we are motivated to investigate the binding behaviors of coralyne with triplex DNA by ultrafast time-resolved fluorescence (TRF) spectroscopy method. Three representative triplex structures with oligonucleotide sequences, respectively, containing CGG, CGC⁺, and TAT segments are selected, as shown in Scheme 1. By monitoring the fluorescence decay dynamics, it is observed that coralyne bound within triplex follows a multiexponential fluorescence decay behavior. For G-containing triplex, the fluorescence lifetime components are markedly shorter than free coralyne and coralyne in pure TAT triplex, due to the electron transfer (ET) process between the excited singlet state of coralyne and the G bases in the triplex. The lowest oxidation potential of G base renders it as the most active

electron donor to incur ET with the excited singlet state of coralyne, whereas ET is not feasible for other bases (A, T, and C). From the multiexponential fluorescence lifetimes, the coexisting binding modes of monomeric coralyne (full and partial) intercalation and aggregate coralyne stacking along the phosphate backbone are allowed to be explicitly differentiated, and their respective contributions to the overall binding are determined. For coralyne in the antiparallel CGG triplex, three binding modes are found to exist simultaneously, and monomeric (full and partial) intercalation is predominant. In contrast, in the parallel CGC⁺ triplex, full intercalation is absent, and backbone binding of coralyne aggregate becomes the dominant binding mode due to the charge repulsion between protonated cytosine and cationic coralyne. Furthermore, melting temperature measurements confirm that owing to the stronger π - π interaction between fused-aromatic-ring structure of coralyne and triplex base-triplets, the monomeric intercalation can improve the stability of triplex structure significantly. These results provide in-depth mechanistic insights for understanding the remarkable propensity of coralyne in selective binding to triplex DNA structures and prospective applications of coralyne-triplex targeted anti-gene therapeutics.

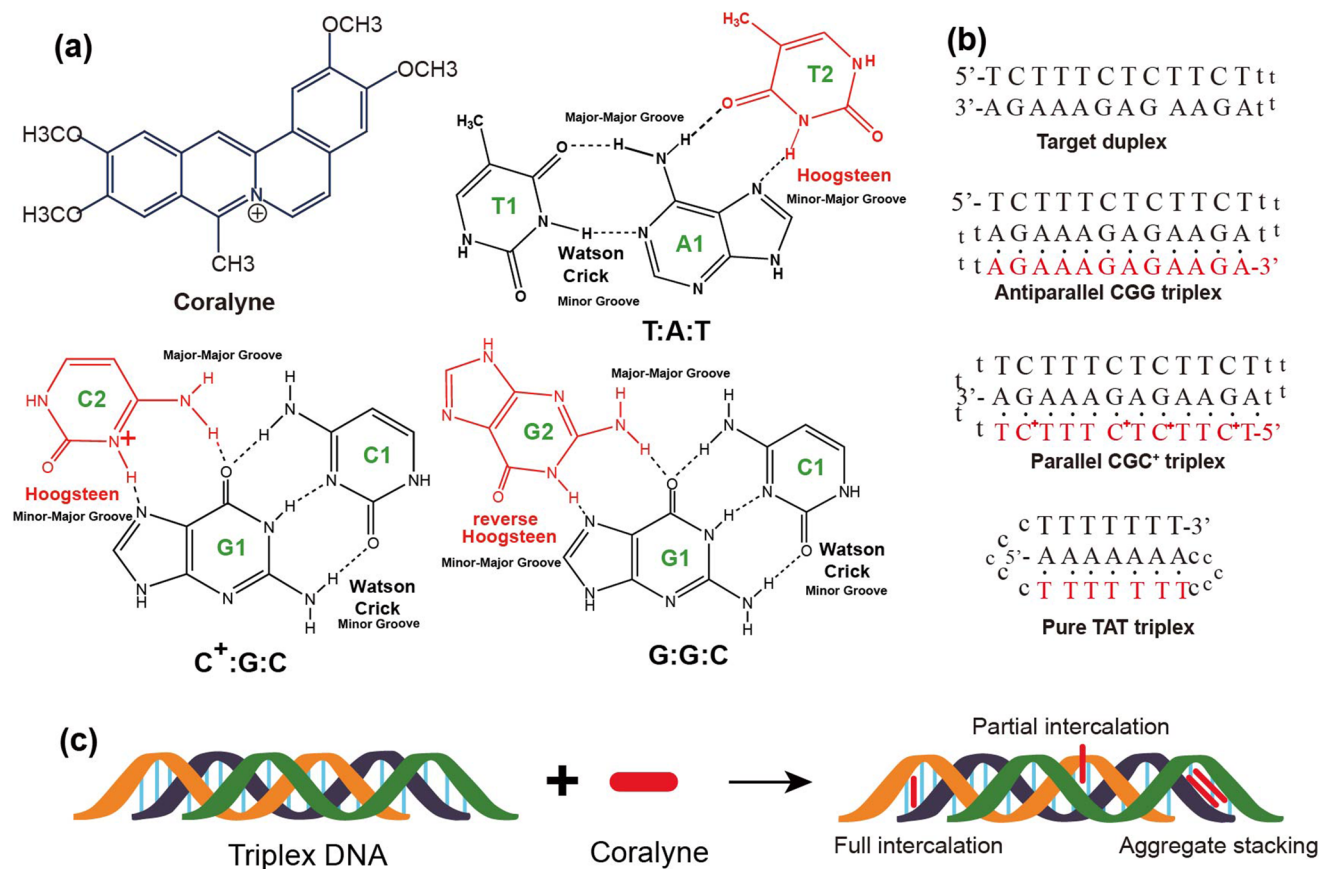
II. MATERIALS AND METHODS

A. Materials

Coralyne, in the form of chloride salt, was purchased from Sigma-Aldrich. Sodium phosphate was purchased from Beijing Shiji. The DNA oligonucleotides of antiparallel triplex, parallel triplex, TAT triplex, and target duplex (Scheme 1) were purchased from Sangon Biotech (Shanghai) Co., Ltd. in ULTRAPAGE-purified form. The concentration of coralyne was estimated from absorbance measurements using the molar absorption coefficient, $\epsilon = 14\,500\text{ M}^{-1}\text{ cm}^{-1}$ at λ_{max} of 420 nm.²³ Single-strand DNA concentrations were determined by monitoring the absorbance at 260 nm in the UV-Vis spectra, and the corresponding extinction coefficients of 446 100, 396 500, 271 100 and 270 500 $\text{M}^{-1}\text{ cm}^{-1}$, for antiparallel CGG triplex, parallel CGC⁺ triplex, pure TAT triplex, and target duplex, respectively, were obtained from <https://www.idtdna.com>. The four DNAs were prepared as follows: The oligonucleotide samples were dissolved in 100 mM sodium phosphate buffer solution at pH 7.5 for antiparallel CGG triplex, pure TAT triplex, and target duplex, as well as 100 mM sodium phosphate buffer solution at pH 5.0 for parallel CGC⁺ triplex. The oligonucleotide samples were then heated to 90 °C for 10 min before they were cooled down to room temperature with a cooling rate of 0.5 °C/min and incubated at 4 °C overnight. The formation of triplex DNA was confirmed by its characteristic circular dichroism (CD) spectra pattern and biphasic optical melting profile, and these were consistent with earlier reports.^{24,25} All the reagents were used as received.

B. Steady-state spectral measurements

(a) Circular dichroism experiments were performed at room temperature using a ChirascanTM Circular Dichroism spectrometer (Applied Photophysics Ltd., Surrey, United Kingdom). Each measurement was recorded from 200 to 400 nm at a scanning rate of 100 nm/min. The final data were the average of three



Scheme 1. (a) Molecular structure of coralyne, base-triplets of TAT, CGC⁺, and CGG in three triplex; (b) the oligomer sequences of the target duplex, antiparallel CGG triplex, parallel CGC⁺ triplex, and pure TAT triplex, as well as their folding style; and (c) the sketch of proposed binding modes of coralyne with triplex.

measurements. The scan of the buffer alone was used as the background, which was subtracted from the average scan for each sample. (b) Fluorescence spectra were measured with a fluorescence spectrometer (F4600, Hitachi) at the excitation wavelength of 350 nm. Quartz cuvettes with a 1 cm path length were used for all steady-state spectral measurements. The oligonucleotide concentrations were 9 μM , and the coralyne concentration was 3 μM .

C. Absorption spectra titrations

UV-Vis absorption spectra were recorded in the wavelength range of 200–800 nm with a UV-Vis spectrometer (model U-3900, Hitachi). Absorption spectra titrations were carried out at room temperature to determine the binding affinity between DNA and coralyne. Initially, 2000 μl solutions of the blank buffer and the coralyne sample (5 μM) were placed in the reference and sample cuvettes (1 cm path length), respectively, and then the first spectrum was recorded in the range of 220–500 nm. During the titration, an aliquot (5 μl) of buffered DNA solution (200 μM) was added to each cuvette to eliminate the absorbance of the DNA itself, and the solutions were mixed by repeated inversion. After the solutions

were mixed for ~ 10 min, the absorption spectra were recorded. The titration processes were repeated until there was no change in the spectra for at least four titrations, indicating binding saturation had been achieved. The changes in the coralyne concentration due to dilution at the end of each titration were negligible. The intrinsic binding constants K_b were obtained using the following Eq. (1):²⁶

$$(\varepsilon_a - \varepsilon_f)/(\varepsilon_b - \varepsilon_f) = (b - (b^2 - 2K_b^2 C_t [\text{DNA}]/s)^{1/2})/2K_b C_t, \quad (1a)$$

$$b = 1 + K_b C_t + K_b [\text{DNA}]/2s, \quad (1b)$$

where [DNA] is the concentration of the base-pair, ε_a , ε_f , and ε_b are the apparent extinction coefficients ($A_{\text{abs}}/[\text{Coralyne}]$), the extinction coefficient for free coralyne, and the extinction coefficient for coralyne in the fully bound form, respectively. Here ε_b is determined when the concentration ratio $[\text{DNA}]/[\text{coralyne}] = 3:1$. K_b is the equilibrium binding constant in M^{-1} , C_t is the total coralyne concentration, and s is the binding size of the small molecule interacting with DNA.

D. UV thermal denaturation experiments

Thermal DNA denaturation experiments were carried out with a UV-Vis spectrometer (model U-3500, Hitachi) equipped with a temperature-control programmer ($\pm 0.1^\circ\text{C}$). Melting curves were collected by UV absorbance as a function of temperature. The temperature of the solution was increased from 5 to 90°C at a rate of $1^\circ\text{C}/\text{min}$, and the absorbance at 260 nm was continuously monitored for solutions of DNA in the absence and presence of the coralyne.^{25,27} The oligonucleotide concentrations were $5\ \mu\text{M}$, and the coralyne concentration was $15\ \mu\text{M}$. Quartz cuvettes of 1 cm path length were used for all UV-thermal denaturation measurements.

E. Time-resolved fluorescence measurements

Time-resolved fluorescence spectra were measured using a high-resolution streak camera system: the Universal Streak Camera (C10910-05, Hamamatsu) combined with a CMOS camera (C13440-20CU) and a spectrometer (HRS-300-S). The camera had two time sweep regimes: fast (minimum time window, 70 ps) and slow (minimum time window, 1 ns). The maximum temporal resolution of the streak camera in the single-pulse regime was 1.37 ps. In our experiments, the time-resolved fluorescence spectra and dynamics on the 200 and 1200 ps were collected through the fast sweep regime, and the time-resolved fluorescence spectra and dynamics on the 20 and 50 ns time scales were collected through the slow sweep regime. The fs 350 nm pump beam was generated from the optical parametric amplifier (TOPAS-C, Coherent Inc.). The fundamental pulse (800 nm, 40 fs, and 1 kHz repetition rate) was generated with a Ti:Sapphire laser system (Coherent Astrella). Sample solutions were in

a 1 mm fused silica cuvette, and the sample cell was continuously moved to avoid photodamage.

III. RESULTS AND DISCUSSION

A. Steady-state spectra of coralyne and coralyne bound to DNA

We chose two representative triplex oligonucleotide sequences: an antiparallel CGG triplex containing pyrimidine-purine-purine segments and a parallel CGC⁺ triplex containing pyrimidine-purine-pyrimidine segments. These two sequences can fold back twice on themselves and form an intramolecular triplex, in which the third strand would adopt an antiparallel orientation or a parallel orientation with respect to the homologous purine strand of the target duplex, as shown in Scheme 1(b). Specifically, in the pH 7.5 sodium phosphate buffer solution, the 3'-terminal purine segment of the antiparallel CGG triplex folds back via the tttt loop and pairs with the homologous purine strand of the target duplex by the reversed Hoogsteen hydrogen bonds, forming the CGG and TAA motifs. For the parallel CGC⁺ triplex, the 5'-terminal pyrimidine segments (C base) are partially protonated in the pH 5.0 sodium phosphate buffer solution and can fold back to pair with the homologous purine strand of the target duplex by Hoogsteen hydrogen bonds, forming C⁺GC and TAT motifs.²⁴

Figure 1 shows the CD spectra measured here for the antiparallel CGG triplex, the parallel CGC⁺ triplex, and their target duplex at room temperature. Specifically, the CD spectra of the antiparallel CGG triplex display two positive bands (280 and 223 nm) and one negative band (248 nm), and the 223 nm positive band relative to 280 nm has increased intensity compared to that of the target

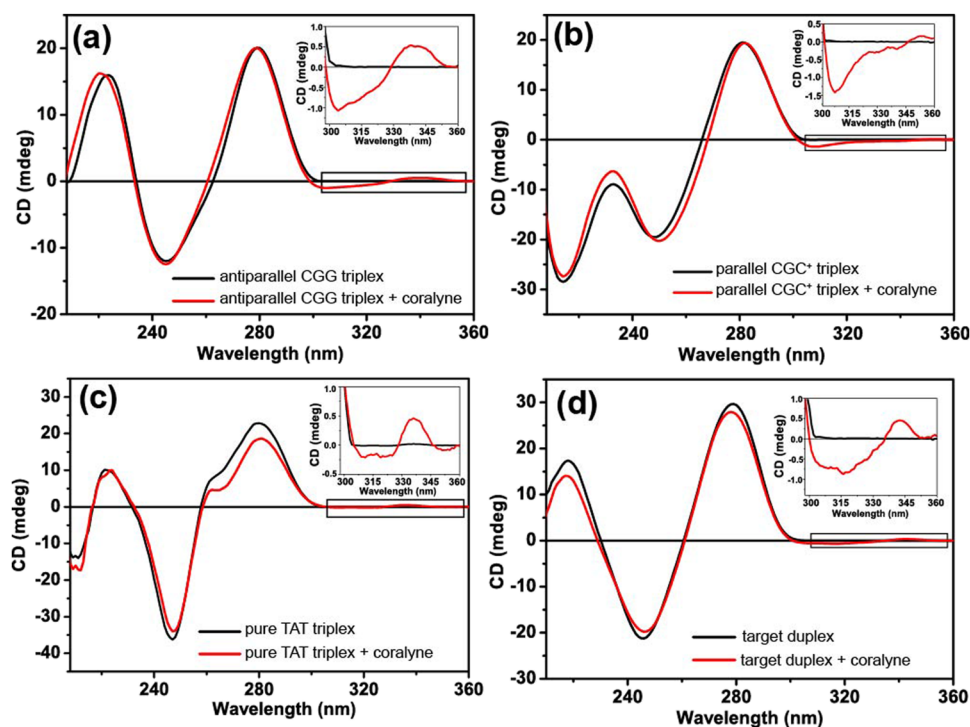


FIG. 1. CD spectra for (a) antiparallel CGG triplex, (b) parallel CGC⁺ triplex, (c) pure TAT triplex, and (d) target duplex in the absence and presence of coralyne ($3\ \mu\text{M}$) in 100 mM sodium phosphate buffer solution. The inset is a magnified view of the signature bump between 300 and 360 nm induced by coralyne intercalation into DNA.

duplex. For parallel CGC⁺ triplex, the positive band at 280 nm and the negative band at 248 nm are still observed, while the positive band at 223 nm is replaced by the emerging negative band at 215 nm. Another triplex DNA containing pure TAT segments will be used in the reference experiment,²⁸ which shows a characteristic CD signal consisting mainly of three positive peaks located at 280, 262 nm (shoulder peak), and 222 nm, as well as two negative peaks at 248 and 211 nm. They are consistent with previous results and demonstrate the formation of the anticipated triplex structures.^{24,28}

After addition of coralyne, the CD spectra of the triplex/coralyne complex display bisignate-induced CD (ICD) bands between 300 and 360 nm, indicating the binding of coralyne into the chiral environment of triplex, as shown in Fig. 1 insets.^{18,22} The ICD signal as reflected by the intensity of the 340 nm positive band relative to the 310 nm negative band is particularly more obvious for the antiparallel CGG triplex and pure TAT triplex [Figs. 1(a) and 1(c)] than the cases of parallel CGC⁺ triplex and target duplex [Figs. 1(b) and 1(d)], consistent with the binding affinity measured by the binding constants below.

Furthermore, the binding of coralyne to triplex is also confirmed by the UV-Vis absorption spectral experiments. As seen in Fig. 2, the spectrum of coralyne alone shows strong absorption in UV (<340 nm) and two well-resolved maxima in visible (at 405 and 420 nm). Upon successive addition of triplex DNA to coralyne, the absorption spectra change significantly, which involves a sharp change (from the black dotted line to the red line in Fig. 2) of redshift and hypochromicity and then a gradual change (from the red line to the purple line in Fig. 2) of absorption intensity increase on continued addition of DNA. The spectra do not display an isobestic point, indicating that there exists more than one binding

conformation of coralyne-DNA. At high coralyne/DNA ratios, the excess coralyne tends to aggregate along the DNA phosphate backbone, as evidenced by the merging of two UV absorption peaks of ~410 and ~430 nm into a broad peak at 420 nm.²⁹ However, at low coralyne/DNA ratios, when coralyne monomer intercalation into DNA base-pairs becomes dominant, the broad peak is split again into two peaks at ~410 and ~430 nm, and the relative intensity of ~430 nm is stronger than that of ~410 nm.²⁹ The electronic absorption spectra are quite different for unbound, stacked aggregate, and intercalated monomer coralyne. Here, for antiparallel CGG and parallel CGC⁺ triplex with the same base-triplet numbers, it is observed that the content of DNA-induced coralyne aggregation in the parallel CGC⁺ triplex is larger than that of the antiparallel CGG triplex, as demonstrated by the merged broad peak of 420 nm [red line in Fig. 2(b) compared to Fig. 2(a)].

Using the UV-Vis absorption spectra change at 334 nm, the apparent binding constants of coralyne with triplex are determined [$6.0 \times 10^6 \text{ M}^{-1}$ for antiparallel CGG and $4.0 \times 10^6 \text{ M}^{-1}$ for parallel CGC⁺, as shown in Figs. 2(a) and 2(b) insets]. By comparison, it shows that coralyne has a stronger binding to the antiparallel CGG triplex than that of the parallel CGC⁺ triplex. Additionally, the binding constants of coralyne with pure TAT triplex ($6.5 \times 10^6 \text{ M}^{-1}$) and target duplex ($1.2 \times 10^6 \text{ M}^{-1}$) are also measured [Figs. 2(c) and 2(d) insets]. Collectively, these data demonstrate a several-fold stronger propensity for coralyne binding with a triplex structure than with a duplex structure.²¹

To examine the stabilization effect of triplex by coralyne binding, thermal UV absorption spectral experiments of DNA in the absence and presence of coralyne are performed by monitoring the absorbance at 260 nm (Fig. 3), which is the characteristic absorption

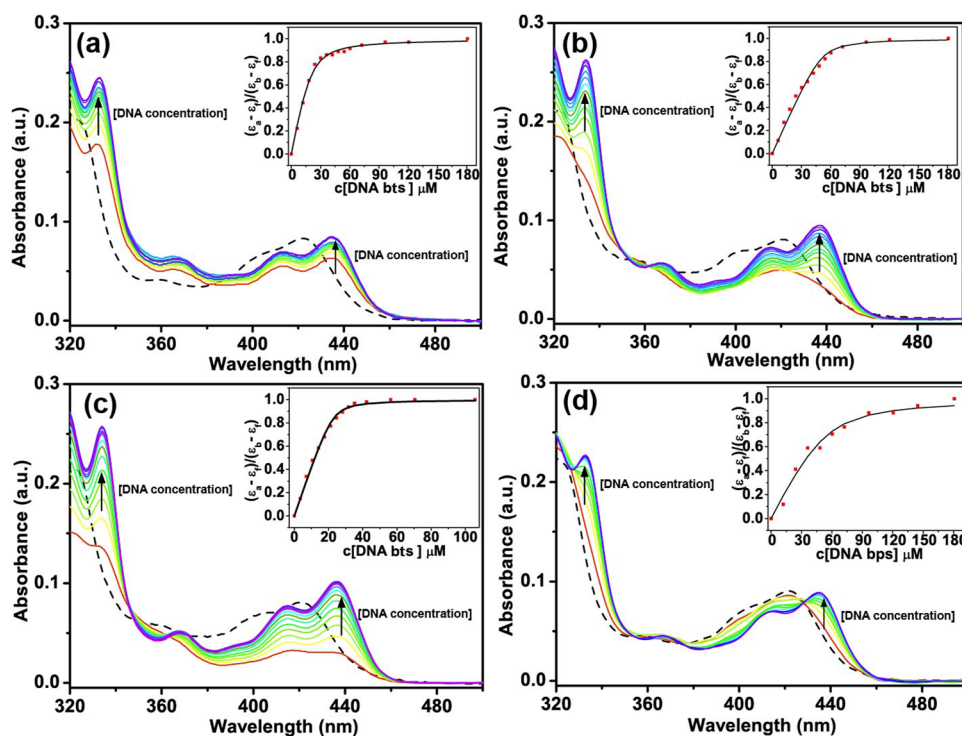


FIG. 2. UV-Vis absorption spectra of 5 μM coralyne (black dotted line) and 5 μM coralyne with increasing amounts of DNA (colorful lines) in 100 mM sodium phosphate buffer solution. (a) coralyne in an antiparallel CGG triplex, (b) coralyne in a parallel CGC⁺ triplex, (c) coralyne in a pure TAT triplex, and (d) coralyne in a target duplex. Inset: Determination of the binding constant (K_b) by measuring $(\epsilon_a - \epsilon_f)/(\epsilon_b - \epsilon_f)$ as a function of DNA base-triplets (bts) or base-pairs (bps) concentration, including a fit line (black line), where ϵ_a , ϵ_f , and ϵ_b are the apparent extinction coefficient (DNA/coralyne), the extinction coefficient of free coralyne, and the extinction coefficient of coralyne in the fully bound form, respectively.^{26,30} The fitted line is obtained from Eq. (1), representing the source of K_b .

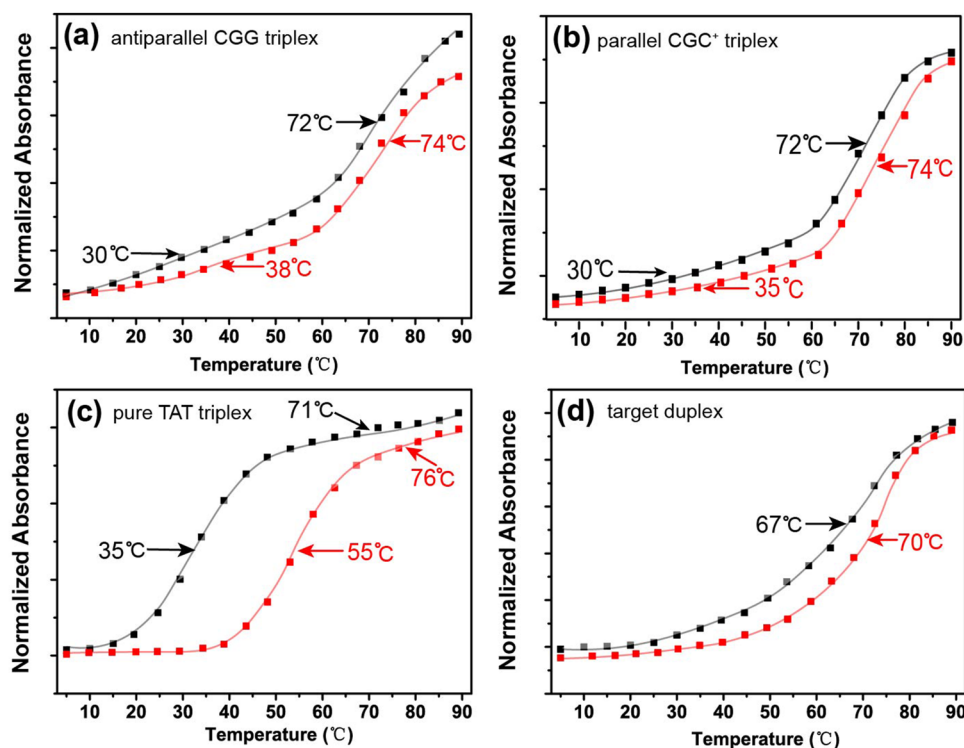


FIG. 3. UV-Vis melting curves for (a) antiparallel CGG triplex, (b) parallel CGC⁺ triplex, (c) pure TAT triplex, and (d) target duplex in the absence (black line) and presence (red line) of coralyne (15 μM). The thermal denaturation temperature of DNA was assessed by the UV absorption signal at 260 nm.

wavelength of DNA. For the triplex DNA [Figs. 3(a)–3(c)], the melting curve exhibits two transition temperatures, which correspond to the transition processes of the triplex to the duplex (T_{m1} , 30–35 °C) and the duplex to the single strand (T_{m2} , 71–72 °C), demonstrating further the formation of the triplex DNA structure.^{8,25,27} In contrast, the melting curve of target duplex [Fig. 3(d)] only shows one transition temperature (T_m , 67 °C), corresponding to the transformation of duplex to single strand. After the addition of coralyne, the UV melting curves of triplex DNA are shifted to higher temperatures, with a significant increase in the T_{m1} ($\Delta T_{m1} \sim 5\text{--}8$ °C) and T_{m2} ($\Delta T_{m2} \sim 2$ °C) of the transitions. The increase of T_{m1} and T_{m2} indicates the stabilization of triplex structure by coralyne binding. Moreover, the increase in transition temperature in antiparallel CGG triplex ($\Delta T_{m1} = 8$ °C) is slightly higher than that of parallel CGC⁺ triplex ($\Delta T_{m1} = 5$ °C), consistent with the higher binding affinity of coralyne with antiparallel CGG triplex as evidenced by the measured binding constants above. In addition, it is noted that a profound increase in transition temperature ($\Delta T_{m1} = 20$ °C) for pure TAT triplex is observed upon binding with coralyne, which is in agreement with previous reports.²² Generally, the π -stacking interaction of ligand with base-pair can increase the DNA stability and thus affect the transition temperature of DNA. Thus, the dramatic increase of melting temperature of pure TAT triplex upon binding with coralyne suggests that there is stronger π - π interaction of the intercalated coralyne molecule with TAT base-triplets, owing to the molecular structure of coralyne (four fused aromatic rings) that is more compatible to stack with TAT than CGG or CGC⁺ base-triplets.

B. Steady-state fluorescence spectra of free coralyne and coralyne bound to triplex

Figure 4 shows the fluorescence spectra of free coralyne and its complex with triplex DNA. As can be seen, free coralyne presents an intense emission spectrum from 440 to 680 nm. Upon binding with a triplex containing CGG or CGC⁺ segments, the fluorescence intensity of coralyne is found to be efficiently quenched compared with

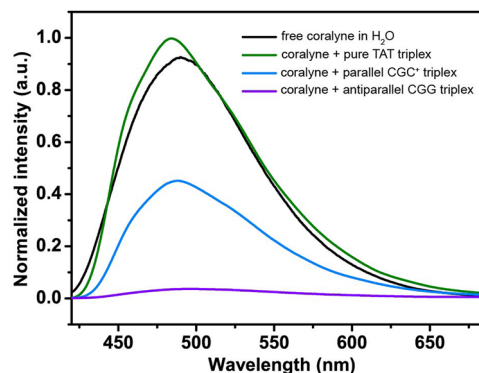


FIG. 4. Steady-state fluorescence emission spectra for free coralyne in water and coralyne bound to pure TAT triplex, parallel CGC⁺ triplex, and antiparallel CGG triplex.

free coralyne. Conversely, the pure TAT triplex displays no quenching effect when bound with coralyne. Generally, it is known that the electron transfer (ET) between the excited state of the photosensitizer and DNA bases can result in efficient fluorescence quenching, particularly for the redox-active bases of guanine (G) and adenine (A).^{31,32} Assuming the excited singlet state of coralyne ($^1\text{coralyne}^*$) is subject to accept an electron from surrounding DNA base, we estimated the standard free energy change (ΔG) of this electron transfer process with four DNA bases based on the Rehm–Weller equation. The reduction potential of coralyne (-0.89 V) is determined from cyclic voltammetry, and the oxidation potentials of nucleobases G ($+1.49$ V), A ($+1.96$ V), T ($+2.11$ V), and C ($+2.14$ V) are from Ref. 33. The excited state energy of $^1\text{coralyne}^*$ is obtained from its fluorescence peak at 472 nm (2.63 eV).³⁴ The estimated driving force shows that the ET between $^1\text{coralyne}^*$ and G base is thermodynamically feasible (-0.25 eV), whereas those of $^1\text{coralyne}^*$ with A, T, and C base are unfavorable, with positive values of 0.22, 0.37, and 0.40 eV, respectively. The calculated ΔG fully agrees with the fluorescence quenching experiments, showing that electron transfer of $^1\text{coralyne}^*$ can only occur with G bases in DNA. Therefore, the fluorescence quenching is only observed for G-containing triplex (Fig. 4). In addition, the possibility of energy transfer contributing to fluorescence quenching has been eliminated due to the lack of spectral overlap between coralyne fluorescence and DNA base absorption.

Interestingly, for the G-containing triplex DNA, a more pronounced fluorescence quenching of coralyne is observed in the antiparallel CGG triplex than that with the parallel CGC⁺ triplex, suggesting a more efficient ET reaction in the antiparallel CGG

triplex. In principle, the relative orientation and distance of the electron donor (D) with respect to the electron acceptor (A) are important factors governing the electron transfer processes in DNA.^{31,32,35,36} Thus, the local microenvironment and binding configuration of coralyne in DNA structures are expected to be crucial for the ET of $^1\text{coralyne}^*$ with G. To further explicitly distinguish binding modes and local microenvironments of coralyne within triplex DNA, we then performed time-resolved fluorescence (TRF) spectroscopy as described below.

C. Ultrafast time-resolved fluorescence spectroscopy for free coralyne and coralyne bound to triplex

Coralyne tends to undergo self-aggregation even in dilute aqueous solutions due to its fused aromatic-ring structure, and the aggregate normally has a longer fluorescence lifetime than the monomer form.³⁷ Given that coralyne aggregation can be circumvented by using 20%–30% (v/v) ethanol (EtOH) as co-solvent and coralyne aggregate will be dissociated to monomer form,³⁸ we performed TRF of coralyne in EtOH/H₂O (30:70, v/v) to obtain the pure fluorescence decay profile of monomer. As shown in Figs. 5(a) and 5(c), the fluorescence decay profile follows a single-exponential decay kinetics with a lifetime of 10.0 ± 0.2 ns (Table I), corresponding to the fluorescence decay lifetime for free coralyne monomer.

As evidenced by steady-state fluorescence emission spectra, pure TAT triplex is unable to quench $^1\text{coralyne}^*$ by ET. Thus, we first measured the TRF spectrum of coralyne in pure TAT

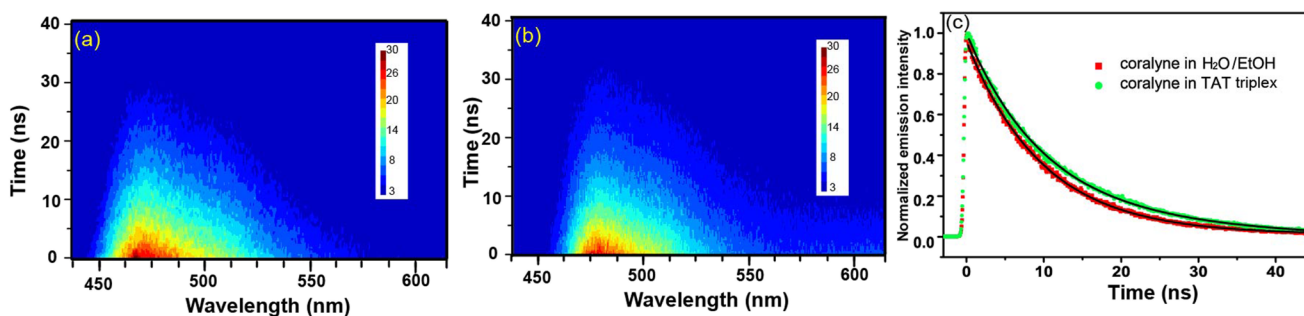


FIG. 5. Time-resolved fluorescence spectra and decay kinetics upon fs 350 nm excitation. Three-dimensional spectra of coralyne ($100 \mu\text{M}$) in (30:70, v/v) EtOH/H₂O (a) and in pure TAT triplex ($300 \mu\text{M}$) of pH 7.5 aqueous phosphate buffer (b); kinetic decay profiles for coralyne ($100 \mu\text{M}$) in H₂O/EtOH and in $300 \mu\text{M}$ pure TAT triplex (c), respectively.

TABLE I. Fluorescence decay lifetimes of free coralyne and coralyne bound with triplex DNA, obtained from monoexponential or multiexponential fittings. Pre-exponential factors for the lifetime components yield the respective percentages of different binding modes (values shown in brackets).

Coralyne in	τ_1 (A ₁ %)	τ_2 (A ₂ %)	τ_3 (A ₃ %)
EtOH/H ₂ O	10.0 ± 0.2 ns		
Pure TAT triplex	9.5 ± 0.3 ns (90%)	31 ± 0.8 ns (10%)	
Antiparallel CGG triplex	12 ± 0.2 ps (47%)	175 ± 3 ps (39%)	3.0 ± 0.1 ns (14%)
Parallel CGC ⁺ triplex	235 ± 7 ps (31%)	7.3 ± 0.2 ns (69%)	

triplex as a reference experiment representing the simple case without the occurrence of ET in DNA. For coralyne in the pure TAT triplex, the fluorescence decay kinetics follow a biexponential law [Figs. 5(b) and 5(c)]. The two fitted fluorescence lifetimes of 9.5 ± 0.3 ns (90%) and 31 ± 0.8 ns (10%) are comparable to those of coralyne monomer (9.7 ns) and aggregate (41 ns) in water, as reported by the previous study.³⁷ Considering the large excess of triplex (3:1M ratio of DNA/ligand) and the high binding constants ($>10^6$ M⁻¹, Fig. 2) of coralyne with DNA, almost all coralyne molecules should bind to triplex. According to previous reports, the monomeric coralyne binds with DNA by intercalation within the base-triplet region, while the bulky aggregate of coralyne can only bind around the phosphate backbone.^{14,16,22} Therefore, the short lifetime (9.5 ns) is assigned to the monomeric coralyne in intercalation mode, and the long lifetime (31 ns) is assigned to the aggregate coralyne stacking along the phosphate backbone. In the biexponential fitting equation, the pre-exponential factors obtained for the two lifetime components are actually related to the respective percentages of two binding modes, and these values are listed in Table I (in brackets). It is shown that for coralyne bound to pure TAT triplex, the percentage of monomeric coralyne is dominant (90%) and the percentage of aggregate coralyne is dramatically decreased (10%) concomitantly, suggesting that coralyne binds with pure TAT triplex mainly by monomeric intercalation within the TAT base-triplets and there is only a small amount of coralyne aggregate bound to the phosphate backbone. This quantitative information is unknown before and could not possibly be obtained by conventional techniques. Moreover, considering that the intercalated monomer of coralyne would adopt strong π - π interaction

with TAT base-triplets, the data obtained here can further rationalize the significant stabilization effect of coralyne on the pure TAT triplex structure as indicated by melting temperature change ($\Delta T_{m1} = 20^\circ\text{C}$).

When coralyne binds to an antiparallel CGG triplex, the fluorescence decay behavior becomes markedly different. As shown in Fig. 6(a), the decay of the TRF spectrum is significantly accelerated. Unlike the dozens of ns-long TRF decays of free coralyne and coralyne in the TAT triplex, the TRF of coralyne in the antiparallel CGG triplex exhibits a decay in the time scale ranging from a picosecond to a few nanoseconds. By combining the overall kinetics of the TRF spectrum on three timescales (200, 1000 ps, and 20 ns), it is observed that the complex dynamics require a best fit by multi-exponentials containing three components with time constants in the tens picoseconds ($\tau_1 = 12 \pm 0.2$ ps), hundred picoseconds ($\tau_2 = 175 \pm 3$ ps), and a few nanoseconds ($\tau_3 = 3.0 \pm 0.1$ ns), as shown in Fig. 6 and Table I, respectively. In detail, the lifetime and percentage of the first component (τ_1) are accurately obtained from the 200 ps timescale [Fig. 6(b) inset], those of the second component (τ_2) are obtained by combining the 200 and 1000 ps timescales [Fig. 6(b)], and those of the third are obtained by combining the 1000 ps and 20 ns timescales [Fig. 6(c)], respectively. The three components of dramatically shorter lifetimes should be attributed to the faster deactivation process of ¹coralyne* bound to this triplex DNA, where a microenvironment and binding configuration are provided that allow photoexcited ¹coralyne* to be quenched by electron transfer (ET) with G base. In this context, the triexponential decay for the bound coralyne should be correlated with the existence of three types of binding configuration.

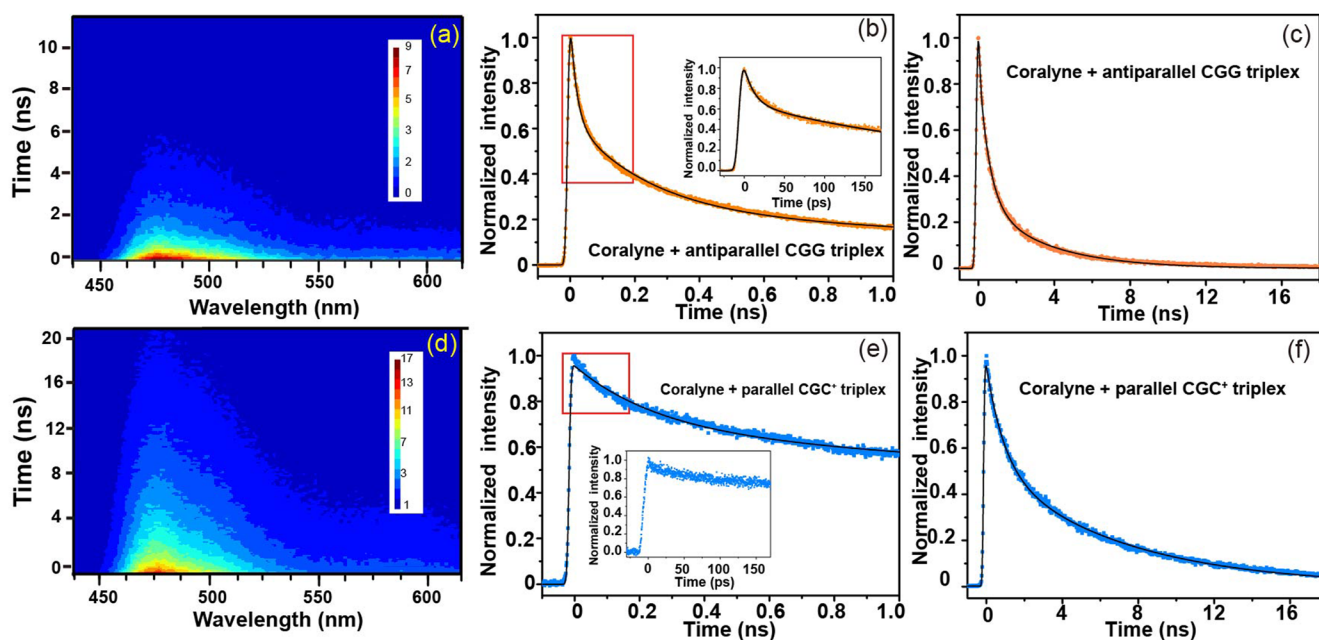


FIG. 6. Time-resolved fluorescence spectra and decay kinetics upon fs 350 nm excitation. Three-dimensional spectra of (a) coralyne (100 μM) in an antiparallel CGG triplex; and (d) in a parallel CGC⁺ triplex, DNA concentration: 300 μM . Kinetic decay profiles for coralyne (100 μM) in two DNAs (300 μM) measured in the time windows of 1000 ps (b) and (e) and 20 ns (c) and (f). The inset: Kinetic decay profiles for coralyne (100 μM) in two DNAs (300 μM) measured in the time window of 200 ps.

As proposed by previous studies^{14,22} and implicated in the electronic absorption spectra measured above (Fig. 2), the binding modes of coralyne may involve monomeric full intercalation or partial intercalation and aggregate stacking along the phosphate backbone (Scheme 2). In the full intercalation mode, coralyne monomer fully π -stacks with base-triplets and has a strong electronic coupling with adjacent G base, constituting a configuration favorable for the occurrence of photoinduced electron transfer (PET). For the coralyne monomer partially intercalated into base-triplets, only moderate electronic coupling with G base is expected due to partial π - π stacking. In the third case, bulky coralyne aggregates stack along the DNA phosphate backbone by electrostatic association. Thus, this binding mode allows the least coupling of coralyne with G bases. Obviously, the three binding configurations correspond to different degrees of electronic couplings between the ET donor (G base) and acceptor (¹coralyne*), leading to large differences in ET reactivity. Therefore, the fast decay components of $\tau_1 = 12 \pm 0.2$ ps (47%) and $\tau_2 = 175 \pm 3$ ps (39%) should correspond to the monomer bound in full and partial intercalation modes, respectively, while the slow decay component of $\tau_3 = 3.0 \pm 0.1$ ns (14%) is assigned to the coralyne aggregate bound in the backbone.

This assignment can be further supported by the reference system in pure TAT triplex. For coralyne in pure TAT triplex, no PET occurs, and fluorescence lifetimes are the nascent ones for monomer and aggregate coralyne, from which the percentages of monomeric intercalation (90%) and aggregate stacking (10%) are accurately determined. Using this monomer and aggregate percentage as a benchmark, here in the antiparallel CGG triplex, it is reasonable that two ps lifetimes of τ_1 (47%), and τ_2 (39%) are assigned to PET rates of monomeric intercalation mode (monomer in total of 86%) and the ns lifetime of τ_3 (14%), is assigned to PET rates of aggregate stacking mode.

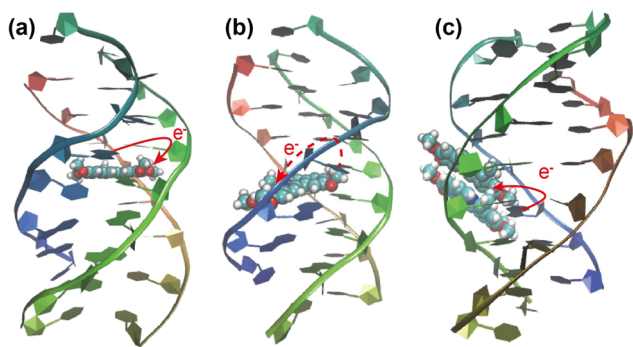
It is worthwhile to mention that in this antiparallel triplex sequence (Scheme 1), whether coralyne monomers stack with a TAA base-triplet or a CGG base-triplet, there are G bases in close proximity, allowing the occurrence of PET. Most likely, there is no preference for coralyne to stack with which base-triplet in this sequence since the surface area of the TAA or CGG triplets is similar.

By monitoring fluorescence decay behaviors, our experiments clearly indicate that three binding modes (full and partial

base-triplets intercalation of monomer and backbone binding of aggregate) simultaneously exist for coralyne interacting with an antiparallel CGG triplex. The scenario of mixed interaction modes and their respective contributions to the coexisting binding modes for coralyne with triplex DNA is thus readily and clearly revealed for the first time. It is also demonstrated that the PET reactivity of coralyne with G base is quite sensitive to the local binding configurations of triplex DNA, allowing easy recognition of different binding modes in a single measurement.

In comparison to coralyne in an antiparallel CGG triplex, the TRF of coralyne in a parallel CGC⁺ triplex exhibits a slower decay profile in the time scale ranging from a hundred picoseconds to twenty nanoseconds and a broader fluorescence emission band [Fig. 6(d)]. Moreover, the TRF dynamics can be best fit by a biexponential decay with two lifetime components in the hundreds of picoseconds ($\tau_1 = 235 \pm 7$ ps), and nanoseconds ($\tau_2 = 7.3 \pm 0.2$ ns), as shown in Figs. 6(e) and 6(f) and Table I, respectively. In particular, the lifetime and percentage of first component (τ_1) are accurately obtained from 1000 ps timescale [Fig. 6(e)], these of second component (τ_2) are obtained by combining 1000 ps and 20 ns timescales [Fig. 6(f)], respectively. In the 200 ps timescale, the fluorescence intensity is sustained and there is no significant decay, indicating the ultrafast component (~ 12 ps) is absent in parallel CGC⁺ triplex, as shown in Fig. 6(e) inset. These data demonstrate that the binding behaviors of coralyne with parallel CGC⁺ triplex are different from those of antiparallel CGG triplex. The absence of the fastest component ($\tau = \sim 12$ ps) indicates the lack of full intercalation mode in parallel CGC⁺ triplex. The two lifetimes are ascribed to the monomeric partial intercalation into the base-triplet (235 ± 7 ps) (31%), and aggregate binding along the sugar-phosphate backbone (7.3 ± 0.2 ns) (69%), respectively, similar to the case in the antiparallel CGG triplex. It should be noted that the two ET lifetimes (partial monomeric intercalation and aggregate binding) of coralyne in parallel CGC⁺ triplex are both slower than that in antiparallel CGG triplex. This can be explained by the reduced G numbers and the increased ionization potential of G within the CGC⁺ triplet in comparison to the CGG triplet.²⁴ Furthermore, for coralyne in parallel CGC⁺ triplex, the percentage of backbone aggregate binding ($\sim 70\%$) is predominant, which is different from that of the preferred monomeric intercalation in antiparallel CGG triplex.

To address the difference in binding modes for coralyne within the antiparallel CGG and parallel CGC⁺ triplexes, we carefully inspect the constitution of two triplex DNAs. It is noted that the antiparallel triplex consists of CGG segments, while the parallel triplex consists of CGC⁺ segments. The parallel CGC⁺ triplex retains a cationic charge due to the partially protonated C base of the third strand. Considering the positive charge of the N⁺-containing aromatic moiety in coralyne, there should exist a charge repulsion between the CGC⁺ segment and cationic coralyne. Such a charge repulsion may hinder coralyne from fully intercalating within base-triplets, and thus this structure could not prevent aggregation. Instead, most coralyne ($\sim 70\%$) would aggregate and be subjected to electrostatic association with the phosphate backbone. Meanwhile, the remaining coralyne monomer ($\sim 30\%$) can only partially intercalate into the base-triplet region. In our parallel CGC⁺ triplex-forming sequences, there are eight TAT segments and four inserted CGC⁺ segments. In principle, the TAT base-triplets are favorable for



Scheme 2. The sketch of coralyne bound to triplex by full intercalation (a), partial intercalation (b), and aggregate stacking along the DNA phosphate backbone (c).

the intercalation of coralyne by strong π - π interactions, as demonstrated by the results for pure TAT triplex DNA (Table I). However, for coralyne in this parallel CGC⁺ triplex, the full intercalation binding is completely absent, indicating that the electrostatic repulsion between coralyne and CGC⁺ segments is so strong that only a few CGC⁺ segments could thoroughly inhibit the full intercalation of coralyne into the triplex base-triplet region. Even though there is a partial intercalation mode in this parallel CGC⁺ triplex, it is presumed that the partial intercalation occurs with the TAT base-triplet but not with CGC⁺ segments that have strong charge repulsion. Thus, it is suggested that the binding behaviors of coralyne toward triplex DNA could be very sensitive to the positive charge in the triplex.

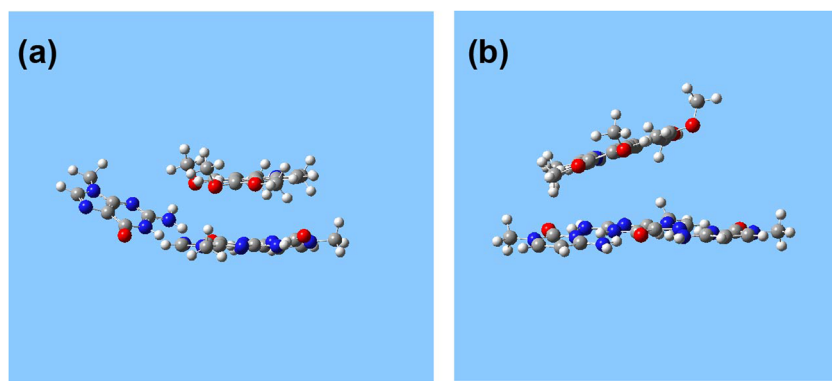
Furthermore, we calculated the electronic coupling between donor and acceptor under well-stacked (CGG) and poor-stacked (CGC⁺) states, which could simplistically represent the full intercalation and partial intercalation binding modes. Based on a two-state model, the fragment charge difference (FCD) method,³⁹ as an extension of generalized Mulliken-Hush method (GMH), can be used to calculate the electronic coupling between a donor site D and an acceptor site A. The FCD analysis of the molecular orbitals is implemented in Multiwfn software.⁴⁰ The electronic density functions are generated by the Gaussian software based on the density functional theory (DFT) method. For coralyne-CGG triplets, the planar structure of coralyne is nearly parallel to CGG base-triplets, and the distance between the donor and acceptor is closer, representing a well-stacked state. In contrast, probably due to the strong electrostatic repulsion, one side of the coralyne structure is tilted and stays far from CGC⁺ base-triplets, resulting in a poor-stacked state, as shown in Scheme 3(b).

The calculated results of electronic coupling (V) for coralyne in well-stacked (CGG) and poor-stacked (CGC⁺) states are 0.0442 and 0.0158 eV, respectively. According to Marcus theory,^{41,42} such different electronic couplings between two states have a noticeable influence on electron transfer rate. Thus, it is expected that for face-to-face acceptor-donor complexes in full intercalation, the electron transfer will be faster than that in partial intercalation mode. The calculated electronic coupling strength for well-stacked is also close to the values reported in previous studies of thionine fully intercalating into DNA (0.0409 eV),⁴³ further supporting our results. Moreover, based on Marcus theory, using the free energy for electron transfer $\Delta G = -0.25$ eV and $\lambda = 1$ eV

(a typical value of the reorganization energy in a polar solvent),^{43,44} we estimated the electron transfer rate of coralyne-CGG triplet in the well-stacked state (7.25 ps) and coralyne-CGC⁺ in the poor-stacked state (56.8 ps). The estimated ratio of rates in the well-stacked and poor-stacked states (i.e., $k_{(\text{well-stacked})}/k_{(\text{poor-stacked})} = 8$) is qualitatively consistent with the measured rate ratio from time-resolved fluorescence experiments ($k_{(\text{full intercalation})}/k_{(\text{partial intercalation})} = 14\text{--}20$). These results could provide a simple model and a basic understanding of the two binding configurations of full and partial intercalation.

Our results corroborate previous studies by steady-state experiments (UV melting, DNase I foot-printing, NMR spectra, etc.), which reported that coralyne preferentially interacts with the pure TAT triplex with six continuous TAT segments, but coralyne binds nearly an order of magnitude less tightly with the alternating TAT/CGC⁺ triplex, where each TAT segment is spaced by one CGC⁺ segment. The chemical shifts observed in NMR supported the intercalation of coralyne in pure TAT triplex. Nevertheless, the weaker binding to the alternating TAT/CGC⁺ triplex was proposed to result in a different conformation, in which the planar coralyne is only partially intercalated, as a consequence of long-range electrostatic interactions between the positively charged ligand and the positive charge on the protonated cytosine.²²

Moreover, we show that in the CGC⁺-containing triplex, the predominant interaction mode becomes the backbone binding of coralyne aggregates. In pure TAT triplex and CGG-containing triplex, coralyne bound to a phosphate backbone also adopts aggregate forms, although with smaller percentages. An intriguing question is thus raised, why does the coralyne bind the DNA phosphate backbone by aggregate stacking instead of monomeric stacking? Is this phenomenon associated with triplex DNA structures? Previous studies have shown that, in comparison to the canonical duplex DNA structure, in the triplex DNA the presence of the third strand widens the major groove and divides it into two asymmetric parts: the minor part of the major groove (mM-groove) and the major part of the major groove (MM-groove), as shown in Scheme 1. Moreover, there exist long-resident water spines with high mobility in MM groove regions, which could significantly alter the water accessibility in the triplex DNA groove and foster a hydrophilic microenvironment.^{24,28,45,46} Therefore, for coralyne bound to the triplex phosphate backbone, the presence of highly mobile hydration waters in the groove region could facilitate the self-aggregation of



Scheme 3. The ground state geometry of coralyne-CGG (a) and coralyne-CGC⁺ (b) optimized at the B3LYP/6-31G* level with the solvent effect simulated by PCM. Carbon, oxygen, nitrogen, and hydrogen atoms are denoted with gray, red, blue, and white balls, respectively.

coralyne. Moreover, the excess negative charge density of the phosphate backbone brought by three-strands in triplex DNA² could reduce the electrostatic repulsion of cationic coralyne molecules and induce coralyne self-aggregation around the backbone (Scheme 2). The specific triplex structure explains well the observations of aggregate stacking binding mode of coralyne. Vice versa, our results indicate that coralyne aggregation is sensitive to the content of water molecules in the local DNA microenvironment and could be used as a probe for recognizing the water content in the local DNA structures.

Overall, our TRF results reveal the sequence-specific binding behavior of coralyne toward triplex DNA. For parallel CGC⁺ triplex, the full intercalation binding is completely absent, and the predominant interaction mode becomes the backbone binding of coralyne aggregates. Indeed, when coralyne interacts with a parallel triplex containing CGC⁺ segments, the binding is a combination of both the electrostatic repulsion of cationic coralyne with protonated cytosine (C⁺) and the electrostatic attraction of cationic coralyne with a negatively charged phosphate backbone. On one hand, although the positive charge of coralyne is localized on the aromatic ring, the charge repulsion of coralyne with protonated cytosine intensely inhibits the monomeric intercalation of coralyne in the parallel CGC⁺ triplex. On the other hand, the electrostatic attraction would facilitate the coralyne aggregate stacking along the DNA phosphate backbone. Affected by two electrostatic interactions, the binding behaviors of coralyne in a parallel CGC⁺ triplex show the absence of monomeric full intercalation and a dominant percentage of backbone binding of coralyne aggregate. For pure TAT triplex and antiparallel CGG triplex when there is no electrostatic repulsion, π - π stacking of coralyne monomer with TAT or CGG base-triplets promotes the monomeric (full and partial) intercalation as the preferred binding mode, whereas aggregate stacking mode accounts for much less percentage. The strong π - π interaction for four-fused-aromatic-ring of coralyne with base-triplets would greatly stabilize the triplex structure, particularly for pure TAT triplex as manifested by the melting temperature measurements.

IV. CONCLUSIONS

In summary, by coupling steady-state spectral measurements and ultrafast time-resolved fluorescence (TRF) spectroscopy, the different binding configurations of coralyne with triplex DNA structures are thoroughly investigated. (1) The steady-state studies show that coralyne has a preferential binding and stabilization for antiparallel CGG and pure TAT triplex over parallel CGC⁺ triplex. (2) Upon binding with G-containing triplex DNA, the fluorescence emission of coralyne is efficiently quenched owing to the photoinduced electron transfer (PET) process of the excited singlet state of coralyne with the G base. (3) By following fluorescence decay kinetics that is sensitive to the binding configuration and local bound microenvironment, coexisting binding modes of coralyne in triplex DNA are explicitly differentiated, revealing monomeric (full and partial) intercalation within base-triplets and aggregate stacking along the phosphate backbone. (4) For coralyne in antiparallel CGG and pure TAT triplex, monomeric (full and partial) intercalation is the preferred binding mode, whereas the backbone binding of coralyne aggregate accounts for a much lower percentage. In contrast, for parallel CGC⁺ triplex, the charge repulsion of

coralyne with protonated cytosine intensely inhibits the full intercalation of monomeric coralyne into base-triplets, and the backbone binding of coralyne aggregates becomes dominant. The DNA-induced coralyne aggregate stacking along the backbone could be associated with the presence of highly mobile hydration waters in groove regions and the excess negative charge density of three-stranded phosphate backbones that promote aggregation, which is unique for triplex structures. These results reveal the π - π stacking and electrostatic interactions that determine the sequence specificity for coralyne binding to triplex DNA. It also shows the ultrafast time-resolved fluorescence as a spectral reporter provides a straightforward and efficient platform to monitor and differentiate the versatile and complex triplex DNA/ligand interactions, which is essential for the application of a triplex-drug complex in targeted anti-gene therapeutics.

ACKNOWLEDGMENTS

This work was financially supported by the National Natural Science Foundation of China (Grant Nos. 21933005, 21727803, 22003005, and 21425313).

AUTHOR DECLARATIONS

Conflict of Interest

The authors have no conflicts to disclose.

Author Contributions

Zeqing Jiao: Conceptualization (equal); Data curation (equal); Formal analysis (equal); Investigation (equal); Methodology (equal); Software (equal); Validation (equal); Visualization (equal); Writing – original draft (equal). **Chunfan Yang:** Formal analysis (equal); Investigation (equal); Software (equal); Visualization (equal). **Qian Zhou:** Investigation (equal); Visualization (equal). **Zheng Hu:** Investigation (equal). **Jialong Jie:** Conceptualization (equal); Formal analysis (equal); Investigation (equal); Validation (equal); Writing – original draft (equal). **Xianwang Zhang:** Investigation (equal). **Hongmei Su:** Conceptualization (equal); Funding acquisition (equal); Project administration (equal); Supervision (equal); Writing – review & editing (equal).

DATA AVAILABILITY

The data that support the findings of this study are available from the corresponding authors upon reasonable request.

REFERENCES

- 1 J. Choi and T. Majima, *Chem. Soc. Rev.* **40**, 5893 (2011).
- 2 I. M. A. Del Mundo, K. M. Vasquez, and G. Wang, *Biochim. Biophys. Acta, Mol. Cell Res.* **1866**, 118539 (2019).
- 3 J. Zhao, A. Bacolla, G. Wang, and K. M. Vasquez, *Cell. Mol. Life Sci.* **67**, 43 (2010).
- 4 G. Wang and K. M. Vasquez, *Mutat. Res.* **598**, 103 (2006).
- 5 M. Duca, P. Vekhoff, K. Oussedik, L. Halby, and P. B. Arimondo, *Nucleic Acids Res.* **36**, 5123 (2008).

- ⁶R. Thenmalarchelvi and N. Yathindra, *Nucleic Acids Res.* **33**, 43 (2005).
- ⁷A. Jain, G. Wang, and K. M. Vasquez, *Biochimie* **90**, 1117 (2008).
- ⁸R. Sinha and G. S. Kumar, *J. Phys. Chem. B* **113**, 13410 (2009).
- ⁹M. D. Keppler, S. Neidle, and K. R. Fox, *Nucleic Acids Res.* **29**, 1935 (2001).
- ¹⁰J. L. Mergny, G. Duval-Valentin, C. H. Nguyen, L. Perrouault, B. Faucon, M. Rougée, T. Montenay-Garestier, E. Bisagni, and C. Hélène, *Science* **256**, 1681 (1992).
- ¹¹C. Escudé, T. Garestier, and J. S. Sun, *Methods Enzymol.* **340**, 340 (2001).
- ¹²P. V. Scaria and R. H. Shafer, *J. Biol. Chem.* **266**, 5417 (1991).
- ¹³S. A. Cassidy, L. Strekowski, W. D. Wilson, and K. R. Fox, *Biochemistry* **33**, 15338 (1994).
- ¹⁴J. S. Lee, L. J. P. Latimer, and K. J. Hampel, *Biochemistry* **32**, 5591 (1993).
- ¹⁵D. S. Pilch, C. Yu, D. Makhey, E. J. LaVoie, A. R. Srinivasan, W. K. Olson, R. R. Sauers, K. J. Breslauer, N. E. Geacintov, and L. F. Liu, *Biochemistry* **36**, 12542 (1997).
- ¹⁶H. Ihmels, K. Faulhaber, D. Vedaldi, F. Dall'Acqua, and G. Viola, *Photochem. Photobiol.* **81**, 1107 (2005).
- ¹⁷B. S. Patro, B. Maity, and S. Chattopadhyay, *Antioxid. Redox Signaling* **12**, 945 (2009).
- ¹⁸Ö. Persil, C. T. Santai, S. S. Jain, and N. V. Hud, *J. Am. Chem. Soc.* **126**, 8644 (2004).
- ¹⁹L.-K. Wang, B. D. Rogers, and S. M. Hecht, *Chem. Res. Toxicol.* **9**, 75 (1996).
- ²⁰D. Makhey, B. Gatto, C. Yu, A. Liu, L. F. Liu, and E. J. LaVoie, *Bioorg. Med. Chem. Lett.* **4**, 781 (1996).
- ²¹J. Ren and J. B. Chaires, *Biochemistry* **38**, 16067 (1999).
- ²²A. Moraru-Allen, S. Cassidy, J.-L. A. Alvarez, K. R. Fox, T. Brown, and A. N. Lane, *Nucleic Acids Res.* **25**, 1890 (1997).
- ²³S. S. Jain, M. Polak, and N. V. Hud, *Nucleic Acids Res.* **31**, 4608 (2003).
- ²⁴Y. Wang, H. Zhao, Q. Zhou, X. Dai, K. Liu, D. Song, and H. Su, *J. Phys. Chem. B* **123**, 2853 (2019).
- ²⁵Y. Kan and G. B. Schuster, *J. Am. Chem. Soc.* **121**, 11607 (1999).
- ²⁶M. T. Carter, M. Rodriguez, and A. J. Bard, *J. Am. Chem. Soc.* **111**, 8901 (1989).
- ²⁷C. Dohno, K. Nakatani, and I. Saito, *J. Am. Chem. Soc.* **124**, 14580 (2002).
- ²⁸Q. Zhou, Y. Wang, X. Dai, C. Yang, J. Jie, and H. Su, *J. Chem. Phys.* **152**, 035101 (2020).
- ²⁹W. D. Wilson, A. N. Gough, J. J. Doyle, and M. W. Davidson, *J. Med. Chem.* **19**, 1261 (1976).
- ³⁰C. Yang, Q. Zhou, Z. Jiao, H. Zhao, C.-H. Huang, B.-Z. Zhu, and H. Su, *Commun. Chem.* **4**, 68 (2021).
- ³¹J. Choi, J. Park, A. Tanaka, M. Park, Y. Jang, M. Fujitsuka, S. Kim, and T. Majima, *Angew. Chem., Int. Ed.* **52**, 1134 (2013).
- ³²S. Paul and A. Samanta, *J. Phys. Chem. B* **122**, 2277 (2018).
- ³³C. A. M. Seidel, A. Schulz, and M. H. M. Sauer, *J. Phys. Chem.* **100**, 5541 (1996).
- ³⁴K. Bhadra and G. S. Kumar, *Biochim. Biophys. Acta* **1810**, 485 (2011).
- ³⁵J. Chen and B. Kohler, *J. Am. Chem. Soc.* **136**, 6362 (2014).
- ³⁶P. Changenet-Barret, T. Gustavsson, D. Markovitsi, and I. Manet, *ChemPhysChem* **17**, 1264 (2016).
- ³⁷M. Megyesi, L. Biczók, and H. Görner, *Photochem. Photobiol. Sci.* **8**, 556 (2009).
- ³⁸H. Ihmels and A. Salbach, *Photochem. Photobiol.* **82**, 1572 (2006).
- ³⁹A. A. Voityuk and N. Rösch, *J. Chem. Phys.* **117**, 5607 (2002).
- ⁴⁰T. Lu and F. Chen, *J. Comput. Chem.* **33**, 580 (2012).
- ⁴¹R. A. Marcus, *J. Chem. Phys.* **43**, 679 (1965).
- ⁴²E. Vauthey, *J. Phys. Chem. B* **126**, 778 (2022).
- ⁴³G. D. Reid, D. J. Whittaker, M. A. Day, D. A. Turton, V. Kayser, J. M. Kelly, and G. S. Beddard, *J. Am. Chem. Soc.* **124**, 5518 (2002).
- ⁴⁴K. Steenkeste, M. Enescu, F. Tfibel, M. Perrée-Fauvet, and M.-P. Fontaine-Aupart, *J. Phys. Chem. B* **108**, 12215 (2004).
- ⁴⁵V. Mohan, P. E. Smith, and B. M. Pettitt, *J. Am. Chem. Soc.* **115**, 9297 (1993).
- ⁴⁶V. Mohan, P. E. Smith, and B. M. Pettitt, *J. Phys. Chem.* **97**, 12984 (1993).